Corrosion Passivation of Gold by *n*-Alkanethiol Self-Assembled Monolayers: Effect of Chain Length and End Group

Francis P. Zamborini and Richard M. Crooks*

Department of Chemistry, Texas A&M University, P.O. Box 300012,
College Station, Texas 77842-3012

Received October 14, 1997. In Final Form: April 9, 1998

Electrochemistry, FTIR-external reflection spectroscopy (FTIR-ERS), and scanning tunneling microscopy (STM) were used to study the ability of *n*-alkanethiol self-assembled monolayers (SAMs) to protect Au from corrosion in aqueous Br^- solutions. The thickness and terminal functional group of the SAMs were varied to determine which factors lead to the greatest corrosion passivation. SAMs prepared on Au from the following molecules were studied: $HS(CH_2)_{15}CH_3$, $HS(CH_2)_{11}CH_3$, $HS(CH_2)_{10}COOH$, and $HS(CH_2)_{11}OH$. The data reveal that, prior to corrosion, the SAMs are crystalline and highly ordered but that afterward they are disordered and oriented parallel to the surface plane. The results show that, for SAMs containing the same terminal functional group, corrosion resistance increases as the SAM thickness increases. For SAMs that are equal in thickness but contain different terminal functional groups, the end groups resulting in the most corrosion resistance follow the order OH > COOH > CH_3. The hydrophilic SAM-modified Au surfaces corrode smoothly in a layer-by-layer fashion while the methyl-terminated, hydrophobic SAM-modified surfaces undergo localized corrosion (pitting). Since hydrophilic SAMs are generally more defective than methyl-terminated SAMs but provide the Au more protection, we conclude that initial SAM defectiveness is not a reliable predictor of its barrier properties.

Introduction

We report a spectroscopic, electrochemical, and scanning tunneling microscopic (STM) study aimed at obtaining a better understanding of the corrosion passivation properties of *n*-alkanethiol self-assembled monolayers (SAMs). Previously we used electrochemical scanning tunneling microscopy (ECSTM) to compare the CN^--induced corrosion of naked Au and Au modified with a hexadecyl mercaptan (C15CH$_3$) SAM.[1] In a more recent study, we found that passivation of Au oxidation by a C15CH$_3$ SAM is markedly improved by underpotentially depositing (UPD) Cu on the Au prior to SAM adsorption.[2] Here, we extend these studies by examining the effect of the *n*-alkanethiol chain length and terminal functional group on corrosion passivation of Au in acidic Br^- solutions.

Au is a noble metal and resistant to corrosion under many circumstances. However, it will dissolve under appropriate chemical or electrochemical conditions in solutions containing complexing agents that shift the dissolution potential sufficiently negative. These include Cl^-, Br^-, I^-, CN^-, and $CS(NH_2)_2$.[3,4] The corrosion of Au is of interest in medicine[5] and the metal plating industry,[3] where it is often used as an anode. Au corrosion is also important to the electronics industry because of its use in thin-film applications and in integrated-circuit technology.[4,6] Halide salts are the most likely candidates for causing Au corrosion in technologically relevant situations; therefore, we chose to study Au in Br^--containing solutions.

Organomercaptan SAMs hold promise as protective coatings because they form thin, highly crystalline barrier films on the coinage metals,[7,8] other metals such as Fe[9] and Pt,[10] and some semiconductors.[11] Additionally, preparation of SAMs is simple, and because they are on the order of only 2.0-nm thick, they do not significantly alter the appearance or most other characteristics of the substrate. Some drawbacks of SAMs are their relatively low thermal and mechanical stability[1,12−15] and their propensity for containing molecule-sized defects.[16−22] Accordingly, it is important to understand the structural and chemical factors that enhance the protection of metals

---

* To whom correspondence should be addressed. E-mail: crooks@chemvx.tamu.edu. Fax: 409-845-1399. Telephone: 409-845-5629.

(1) Zamborini, F. P.; Crooks, R. M. *Langmuir* **1997**, *13*, 122−126.

(2) Zamborini, F. P.; Campbell, J. K.; Crooks, R. M. *Langmuir* **1998**, *14*, 640−647.

(3) Nicol, M. J. *Gold Bull.* **1980**, *13*, 46−55.

(4) Gallagher, N. P.; Hendrix, J. L.; Milosavljevic, E. B.; Nelson, J. H. *J. Electrochem. Soc.* **1989**, *136*, 2546−2551.

(5) Rao, G. M. *Corros. Sci.* **1990**, *30*, 747−752.

(6) Frankenthal, R. P.; Siconolfi, D. J. *J. Electrochem. Soc.* **1982**, *129*, 1192−1196.

(7) Nuzzo, R. G.; Allara, D. L. *J. Am. Chem. Soc.* **1983**, *105*, 4481−4483.

(8) DuBois, L. H.; Nuzzo, R. G. *Annu. Rev. Phys. Chem.* **1992**, *43*, 437−463.

(9) Kawai, T.; Nishihara, H.; Aramaki, K. *J. Electrochem. Soc.* **1996**, *143*, 3866−3873.

(10) Hines, M. A.; Todd, J. A.; Guyot-Sionnest, P. *Langmuir* **1995**, *11*, 493−497.

(11) Sheen, C. W.; Shi, J.-X.; Martensson, J.; Parikh, A. N.; Allara, D. L. *J. Am. Chem. Soc.* **1992**, *114*, 1514−1515.

(12) Schoer, J. K.; Ross, C. B.; Crooks, R. M.; Corbitt, T. S.; Hampden-Smith, M. J. *Langmuir* **1994**, *10*, 615−618.

(13) Kim, T.; Chan, K. C.; Crooks, R. M. *J. Am. Chem. Soc.* **1997**, *119*, 189−193.

(14) Liu, G.; Salmeron, M. B. *Langmuir* **1994**, *10*, 367−370.

(15) Xu, S.; Liu, G. *Langmuir* **1997**, *13*, 127−129.

(16) Finklea, H. O.; Avery, S.; Lynch, M. *Langmuir* **1987**, *3*, 409−413.

(17) Finklea, H. O.; Snider, D. A.; Fedyk, J. *Langmuir* **1990**, *6*, 371−376.

(18) Chidsey, C. E. D.; Loiacono, D. N. *Langmuir* **1990**, *6*, 682−691.

(19) Creager, S. E.; Hockett, L. A.; Rowe, G. K. *Langmuir* **1992**, *8*, 854−861.

(20) Sun, L.; Crooks, R. M. *Langmuir* **1993**, *9*, 1951−1954.

(21) Chailapakul, O.; Sun, L.; Xu, C.; Crooks, R. M. *J. Am. Chem. Soc.* **1993**, *115*, 12459−12467.

(22) Zhao, X.-M.; Wilbur, J. L.; Whitesides, G. M. *Langmuir* **1996**, *12*, 3257−3264.

S0743-7463(97)01121-9 CCC: $15.00

and other materials by SAMs and to design new, more effective ultrathin coatings.

A number of studies have appeared which examine the properties of SAMs as a function of their chain length and end group. For example, Porter *et al.*[23] used infrared (IR) spectroscopy, ellipsometry, and voltammetry to study the crystallinity and passivating properties of methyl-terminated *n*-alkanethiol SAMs having different chain lengths. They concluded that crystallinity and resistance to ion penetration increase as a function of the SAM thickness. Chidsey and Loiacono[18] studied the dependence of the end group on the defectiveness and permeability of *n*-alkanethiol monolayers of approximately the same thickness. They found that the order from least to most defective was as follows: $CF_3(CF_2)_7(CH_2)_2SH < CH_3(CH_2)_9SH < HOCH_2(CH_2)_{10}SH < NC(CH_2)_{10}SH < HO_2C(CH_2)_{10}SH$. The effectiveness of monolayer blocking, as determined by the resistance to electron transfer, correlated well with the extent of order within alkyl chains inferred by IR data. In contrast to the case for shorter-chain thiols (9−10 CH_2 units) studied by Chidsey, Nuzzo et al. found that, for longer-chain *n*-alkanethiols (15 CH_2 units), the various functional end groups had little effect on the crystallinity of the hydrocarbon chains.[24]

There have been few corrosion studies of surfaces modified with *n*-alkanethiols. Feng et al. studied 1-dodecanethiol SAMs formed on Cu surfaces and found that the corrosion resistance depended on the pretreatment of the Cu.[25] Jennings and Laibinis studied the corrosion of Cu that was modified with CH_3-terminated *n*-alkanethiol SAMs of different thicknesses.[26] On the basis of XPS and contact-angle measurements they determined that the monolayers effectively screen the metal from interaction with water and that thicker SAMs are superior at preventing Cu oxidation. Scherer et al. performed the first in-situ STM corrosion study of Cu(100) surfaces modified with *n*-alkanethiols.[27] They found that the presence of the monolayer shifts the onset for Cu corrosion to more positive potentials and that pits form on the Cu surface during corrosion. Polymerized SAMs[13,28] and modification of SAMs with a covalently linked second layer[29−31] have recently been shown to passivate metal surfaces better than simple linear-chain SAMs.

Here, we examine four different *n*-alkanethiol SAMs adsorbed onto Au: $HS(CH_2)_{11}OH$ (C11OH), $HS(CH_2)_{10}COOH$ (C10COOH), $HS(CH_2)_{11}CH_3$ ($C11CH_3$), and $HS(CH_2)_{15}CH_3$ ($C15CH_3$). All these monolayers shift the corrosion potential of Au in Br^--containing aqueous electrolyte solutions to more positive values compared to those for the naked surface. Longer-chain SAMs protect the metal better than shorter-chain SAMs having identical end groups. Provided the SAM thicknesses are approximately equal, the end groups providing the best protection follow the order OH > COOH > CH_3. The STM results reveal that corrosion of Au modified with OH- and COOH-terminated SAMs proceeds smoothly while pitting occurs on the Au modified with CH_3-terminated SAMs. Clearly there is a complex interrelationship between the extent of substrate corrosion and the SAM thickness and chemical composition and size of the end group.

Experimental Section

Chemicals. $HS(CH_2)_{15}CH_3$ (Aldrich, 92%) and $HS(CH_2)_{11}CH_3$ (Aldrich, 98%) were purified by distillation under reduced pressure. $HS(CH_2)_{10}COOH$ (Aldrich, 95%), $HS(CH_2)_{11}OH$ (Aldrich, 97%), KBr (Aldrich, 99.99%), $HClO_4$ (Seastar, ultrapure), and 100% ethanol were used as received. All electrolyte solutions were prepared with deionized water (Millipore, Milli-Q purification system, resistance $\approx$ 18 MΩ·cm).

Substrate Preparation. Au-coated substrates for FTIR-external reflection spectroscopy (FTIR-ERS) and cyclic voltammetry (CV) were prepared by electron-beam deposition of 10 nm of Ti followed by 200 nm of Au onto Si(100) wafers (Lance Goddard Assoc., Foster City, CA). For convenience, different substrates were used to obtain the FTIR-ERS and CV data shown in the figures, but FTIR-ERS data were also obtained of the SAM-modified substrates used for the CV analysis to ensure the presence and quality of the SAM. The Au-coated Si wafers were cleaned in a low-energy Ar plasma cleaner at medium power for 1 min (Harrick Scientific Corp., New York, Model PDC-32G) before all experiments. Substrates used for STM analysis were prepared as described previously.[12,32−36] Briefly, melting an Au wire (0.5-mm diameter, 99.99% purity, Refining Systems Inc., Las Vegas, NV) in a H_2/O_2 flame yields a 1.5−2.0-mm-diameter ball at the end of the wire. The ball has a few elliptical Au(111) facets (long axis $\sim 300\ \mu m$) on its surface that contain atomically flat terraces up to 1-μm wide. The Au balls were cleaned by soaking in a piranha solution (1:2 H_2O_2/H_2SO_4) for 10−15 min. SAMs were prepared by placing the Au-coated wafers or balls in an ethanolic solution of the organomercaptan (1−2 mM) for >24 h, removing them from solution, rinsing with absolute ethanol, and then drying under a stream of N_2.

FTIR-ERS Measurements. FTIR-ERS measurements were made using a Bio-Rad Digilab FTS-40 spectrometer equipped with a Harrick Scientific Seagull reflection accessory and a liquid-N_2-cooled MCT detector. All spectra were obtained using *p*-polarized light at an 84° angle of incidence with respect to the surface normal. Spectra are the sum of 256 or fewer individual scans. Some of the spectra were baseline corrected with no more than three points.

Electrochemical Measurements. Electrochemical experiments were carried out in a cell fabricated from Kel-F and designed to expose 0.25 cm^2 of the Au-coated wafer defined by a Teflon-coated O-ring. The approximately 15-mL cell volume accommodates a Pt counter electrode and an Ag/AgCl, 3 M NaCl reference electrode (Bioanalytical Systems, West Lafayette, IN), against which all potentials are reported. All electrochemical experiments were performed with a Pine Instruments model AFCBP1 bipotentiostat (Grove City, PA), and the data were recorded on a Kipp and Zonen X−Y recorder. All electrolyte solutions were air-saturated. Potentials cited in the literature were converted from a normal hydrogen electrode to an Ag/AgCl, 3 M NaCl electrode scale by subtracting 0.205 V from the cited value.

STM Measurements. All STM data were acquired in air in constant-current mode using a Nanoscope III scanning tunneling microscope (Digital Instruments, Santa Barbara, CA). The tips were mechanically cut 80/20 Pt/Ir (Digital Instruments, Santa Barbara, CA). The bias (E_b) in all images was 300 mV, and the tunneling current (i_t) was 150 pA. The *z*-range (*z*) and root-mean-square roughness (rmsr) are noted in the figures or figure captions. The corrosion experiments were performed ex situ;

---

(23) Porter, M. D.; Bright, T. B.; Allara, D. L.; Chidsey, C. E. D. *J. Am. Chem. Soc.* **1987**, *109*, 3559−3568.

(24) Nuzzo, R. G.; Dubois, L. H.; Allara, D. L. *J. Am. Chem. Soc.* **1990**, *112*, 558−569.

(25) Feng, Y.; Teo, W. K.; Siow, K. S.; Gao, Z.; Tan, K. L.; Hsieh, A. K. *J. Electrochem. Soc.* **1997**, *144*, 55−64.

(26) Jennings, G. K.; Laibinis, P. E. *Colloids Surf., A* **1996**, *116*, 105−114.

(27) Scherer, J.; Vogt, M. R.; Magnussen, O. M.; Behm, R. J. *Langmuir* **1997**, *13*, 7045−7051.

(28) Kim, T.; Chan, K. C.; Crooks, R. M.; Ye, Q.; Sun, L. *Langmuir* **1996**, *12*, 6065−6073.

(29) Itoh, M.; Nishihara, H.; Aramaki, K. *J. Electrochem. Soc.* **1994**, *141*, 2018−2023.

(30) Itoh, M.; Nishihara, H.; Aramaki, K. *J. Electrochem. Soc.* **1995**, *142*, 3696−3704.

(31) Itoh, M.; Nishihara, H.; Aramaki, K. *J. Electrochem. Soc.* **1995**, *142*, 1839−1846.

(32) Schoer, J. K.; Zamborini, F. P.; Crooks, R. M. *J. Phys. Chem.* **1996**, *100*, 11086−11091.

(33) Hsu, T.; Cowley, J. M. *Ultramicroscopy* **1983**, *11*, 239−250.

(34) Ross, C. B.; Sun, L.; Crooks, R. M. *Langmuir* **1993**, *9*, 632−636.

(35) Snyder, S. R. *J. Electrochem. Soc.* **1992**, *139*, 5C.

(36) Sun, L.; Crooks, R. M. *J. Electrochem. Soc.* **1991**, *138*, L23−L25.

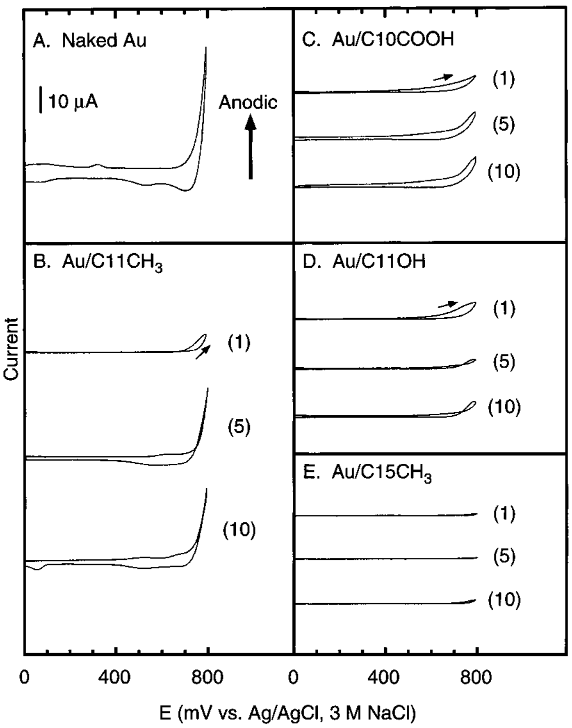

Figure 1. Cyclic voltammograms obtained in an aqueous electrolyte solution containing 10 mM KBr + 0.1 M $HClO_4$ from 0 to 800 mV at 50 mV/s of (A) naked Au, (B) Au/C11CH_3, (C) Au/C10COOH, (D) Au/C11OH, and (E) Au/C15CH_3. The electrode area was 0.25 cm^2.

therefore, the images before and after corrosion were obtained on different regions of the Au ball.

Results and Discussion

Voltammetric Characterization. Figure 1 shows cyclic voltammograms (CVs) of naked Au and the first, fifth, and tenth scans of SAM-modified Au surfaces obtained between 0 and 800 mV at a scan rate of 50 mV/s in an aqueous electrolyte solution containing 10 mM KBr and 0.1 M $HClO_4$. The CV of naked Au is shown in Figure 1A. The principal anodic process, which begins at about 700 mV, arises from Au dissolution (eq 1).[37,38] The first cathodic peak present at approximately 700 mV is due to the reverse process: reduction of $AuBr_2^-$. There is a second and smaller cathodic peak at approximately 530 mV, which corresponds to eq 2.[37,38] The $AuBr_4^-$ species results from the disproportionation of $AuBr_2^-$ on the surface according to eq 3.[39]

$$AuBr_2^- + e = Au + 2Br^- \ (E° = 0.754\ V) \qquad (1)$$

$$AuBr_4^- + 2e = AuBr_2^- + 2Br^- \ (E° = 0.597\ V) \qquad (2)$$

$$3AuBr_2^- = AuBr_4^- + 2Au + 2Br^- \qquad (3)$$

Similar cyclic voltammograms are observed for the SAM-coated electrodes (parts B−E of Figure 1), but the onset of anodic current is shifted to more positive potentials and the magnitude of the current is significantly reduced. Except for the case of the C11CH_3-modified electrode, whose behavior approaches that of naked Au, the SAMs are fairly stable and continue to provide a significant level of passivation even after 10 voltammetric scans. As judged from the voltammetry, the order of corrosion resistance from most to least effective at these small overpotentials is as follows: C15CH_3 > C11OH > C10COOH > C11CH_3.

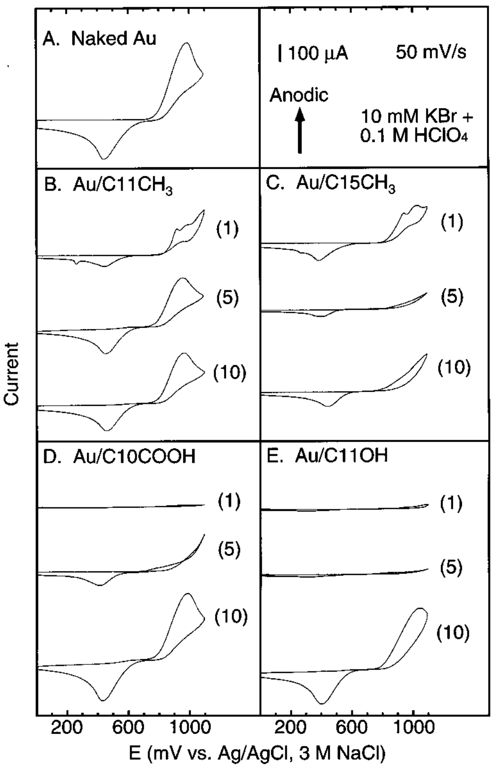

Figure 2. Cyclic voltammograms obtained in an aqueous electrolyte solution containing 10 mM KBr + 0.1 M $HClO_4$ from 0 to 1.1 V at 50 mV/s of (A) naked Au, (B) Au/C11CH_3, (C) Au/C15CH_3, (D) Au/C10COOH, and (E) Au/C11OH. The electrode area was 0.25 cm^2.

These data support the conclusion that longer-chain SAMs passivate the surface more effectively than shorter-chain SAMs and that, for similar thicknesses, monolayers with OH and COOH end groups passivate the surface more effectively than those terminated with a CH_3 group. Other reports have demonstrated that OH- and COOH-terminated SAMs are more defective and less well-packed than CH_3-terminated SAMs, as judged by the extent of molecular penetration through the SAM.[18] Accordingly, we conclude that the number of defects in the SAM does not necessarily correlate strongly with corrosion resistance. This point will be discussed in detail later.

Figure 2 shows cyclic voltammograms of naked Au and the first, fifth, and tenth scans of SAM-modified Au surfaces obtained between 0 and 1.1 V in the same electrolyte solution used to obtain the data shown in Figure 1. Figure 2A shows that at more positive potentials the current arising from corrosion of naked Au increases and that as the potential approaches 1.1 V, the current drops off due to mass-transfer-limited diffusion of Br^- to the Au surface. Another reaction that may contribute to the anodic current observed in Figure 2A is the oxidation of Br^- (eq 4).[37,40] The cathodic peak in the cyclic voltammogram corresponds to redeposition of Au.

$$Br_2(aq) + 2e = 2Br^- \ (E° = 0.882\ V) \qquad (4)$$

---

[37] This value was converted from an NHE to an Ag/AgCl, 3 M NaCl reference electrode by subtracting 0.205 V from the potential given in the accompanying citation.

[38] Evans, D. A.; Lingane, J. J. *J. Electroanal. Chem.* **1963**, *6*, 1−10.

[39] Pesic, B.; Sergent, R. H. *Metall. Trans. B* **1993**, *24B*, 419−431.

[40] Bard, A. J.; Faulkner, L. R. *Electrochemical Methods: Fundamentals and Applications*; John Wiley & Sons: New York, 1980.

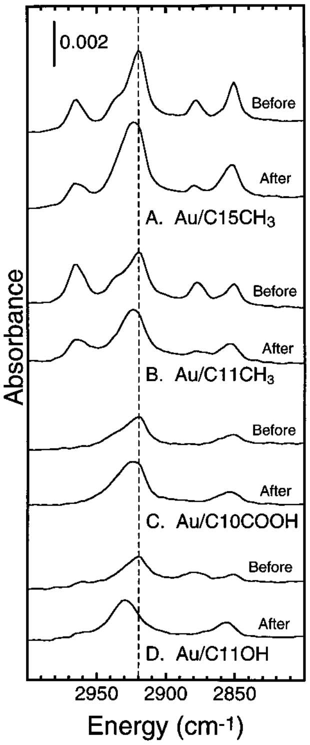

Figure 3. FTIR-ERS spectra of (A) Au/C15CH$_3$, (B) Au/C11CH$_3$, (C) Au/C10COOH, and (D) Au/C11OH before and after corrosion at 800 mV in an aqueous electrolyte solution containing 10 mM KBr + 0.1 M HClO$_4$. The surface was introduced into the electrolyte solution at 0 mV and scanned to 800 mV at 400 mV/s, where it was then held for 2.0 min and emersed under potential control.

At high overpotentials, the C11CH$_3$ and C15CH$_3$ SAMs (Figure 2B and C) show similar blocking ability on the first scan. On subsequent scans Au/C15CH$_3$ becomes more passivating while Au/C11CH$_3$ resembles naked Au. The C11OH and C10COOH SAMs protect Au well for up to five scans, showing superior protection compared to that for the C11CH$_3$ SAM. By the tenth scan, however, these cyclic voltammograms also resemble the cyclic voltammogram of naked Au. It should also be noted that scans obtained after the first scan may be affected by redeposition of Au and that the effect of this process on the SAM is not clear. Nevertheless, it is somewhat surprising that on the first scan the C11OH and C10COOH SAMs protect better than the C15CH$_3$ SAM, since the latter is ~8 Å thicker and terminated with a hydrophobic group.

FTIR-ERS Characterization. Figure 3 shows FTIR-ERS spectra of C15CH$_3$, C11CH$_3$, C10COOH, and C11OH SAMs on Au before and after corrosion at 800 mV in an electrolyte solution identical to that used to obtain the voltammetric data just described. The substrates were introduced into the electrolyte solution at 0 mV and scanned to 800 mV at 400 mV/s. The potential was held at 800 mV for 2.0 min, and then the substrate was emersed at that potential.

The spectra of the SAMs obtained prior to the electrochemical treatment exhibit characteristic asymmetric and symmetric CH$_2$ stretches at 2919−2920 and 2850−2851 cm^{-1}, respectively, indicating a high degree of crystallinity.[18,23,24,41] The Au/C11OH surface (Figure 3D) exhibits a peak at 2879 cm^{-1}, which may be attributed to the C−H stretching mode of the methylene unit adjacent to the OH group.[18,24] Spectra of the CH$_3$-terminated SAMs (Figure 3A and B) reveal asymmetric (2964 cm^{-1}) and symmetric (2936 and 2878 cm^{-1}) CH$_3$ stretches as well. Hydrogen-bonded and non-hydrogen-bonded carbonyl peaks are observed at 1722 and 1741 cm^{-1}, respectively, for the C10COOH monolayer (Figure 4A).[18,24,41−43]

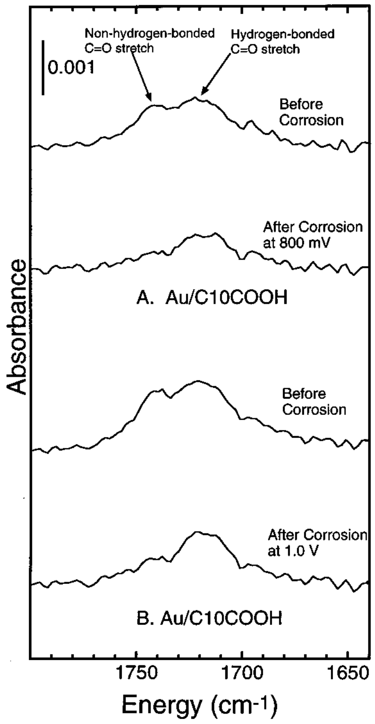

Figure 4. FTIR-ERS spectra of the carbonyl region of Au/C10COOH before and after corrosion at (A) 800 mV for 2.0 min and (B) 1.0 V for 1.0 min in an aqueous electrolyte solution containing 10 mM KBr + 0.1 M HClO$_4$. Run to run reproducibility is represented by the two spectra obtained prior to corrosion.

Spectra of the SAMs obtained after corrosion reveal some definite trends (Figure 3). First, the CH$_2$ modes shift to higher energy by 4−10 cm^{-1} and broaden, which is characteristic of disordering.[23] Second, the asymmetric CH$_2$ stretch increases in intensity, suggesting that the monolayers tilt more parallel to the surface plane.[24,44] Finally, the non-hydrogen-bonded carbonyl peak of the C10COOH monolayer at 1741 cm^{-1} largely disappears after corrosion at 800 mV, but the hydrogen-bonded carbonyl peak at 1722 cm^{-1} remains (Figure 4A). This suggests that C11OH and C10COOH molecules undergoing hydrogen bonding are structurally more stable than non-hydrogen-bonded monolayer components.

Figure 5 shows FTIR-ERS spectra of the C15CH$_3$, C11CH$_3$, C10COOH, and C11OH SAMs on Au before and after corrosion for 1.0 min at 1.0 V in the Br$^-$-containing solution. The positions and the peak widths in the spectra before corrosion again reveal the presence of highly ordered, crystalline monolayers, but the spectra obtained after corrosion are somewhat different than those obtained after scanning the potential to only 800 mV (Figure 3). The asymmetric CH$_2$ stretch of the C15CH$_3$ monolayer shifts to higher energy, indicating disorder, but it decreases in intensity instead of increasing, as it did after corrosion at 800 mV. Another difference is the complete loss of the

---

(41) Sun, L.; Crooks, R. M.; Ricco, A. J. *Langmuir* **1993**, *9*, 1775−1780.

(42) Smith, E. L.; Alves, C. A.; Anderegg, J. W.; Porter, M. D. *Langmuir* **1992**, *8*, 2707−2714.

(43) Kepley, L. J.; Crooks, R. M.; Ricco, A. J. *Anal. Chem.* **1992**, *64*, 3191−3193.

(44) Porter, M. D. *Anal. Chem.* **1988**, *60*, 1143A−1155A.

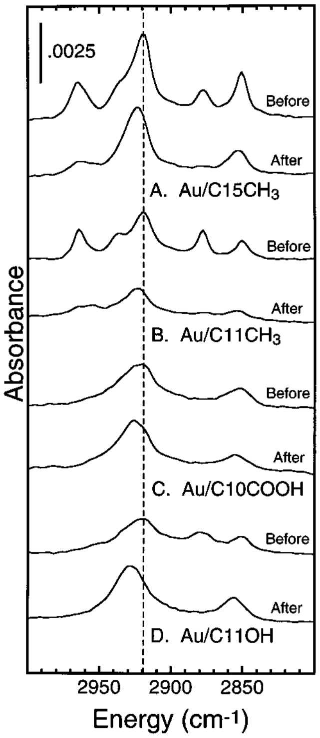

Figure 5. FTIR-ERS spectra of (A) Au/C15CH$_3$, (B) Au/C11CH$_3$, (C) Au/C10COOH, and (D) Au/C11OH before and after corrosion at 1.0 V in an aqueous electrolyte solution containing 10 mM KBr + 0.1 M HClO$_4$. The surface was introduced into the electrolyte solution at 0 mV and scanned to 1.0 V at 500 mV/s, where it was then held for 1.0 min and emersed under potential control.

symmetric CH$_3$ stretch at 2878 cm^{-1}, whereas this peak was still clearly distinguishable after corrosion at 800 mV in Figure 3A. The hydrocarbon stretches of the C11CH$_3$ monolayer are almost completely gone after corrosion at 1.0 V, except for the small asymmetric CH$_2$ band. These results suggest loss of a significant fraction of the methyl-terminated SAMs, not just an orientation change. In contrast, the spectra of the C11OH and C10COOH SAMs show nearly identical changes to the position and intensity of the methylene modes compared to those obtained after corrosion at 800 mV. The spectrum of the carbonyl region of the C10COOH monolayer is also similar (Figure 4B). A control experiment was performed on the Au/C11CH$_3$ and Au/C10C00H surfaces under the same conditions as the experiments represented by Figures 3–5, but in 0.1 M HClO$_4$ solution without the addition of Br$^-$. No significant changes in the IR spectra of any of these surfaces were observed in the absence of Br$^-$. These IR data are consistent with the electrochemical results, which show that C11OH and C10COOH SAMs passivate the Au more effectively than the CH$_3$-terminated SAMs at high overpotentials.

STM Results. Figure 6 shows 3 μm × 3 μm STM images obtained in air of naked Au(111) and SAM-modified Au(111) surfaces under the same conditions used to obtain the FTIR-ERS data presented in Figures 3 and 5. The images before and after corrosion were obtained ex situ and are of different regions of the surface; however, we confirmed that they are representative of the entire surface. Frames A, D, G, J, and M of Figure 6 were obtained before corrosion, and they reveal wide, smooth terraces (>1 μm in width) and Au(111) monatomic steps. The root-mean-square roughness (rmsr) of these surfaces is 0.09–0.10 nm. Frames B, E, H, K, and N were obtained after corrosion at 800 mV for 2 min on different substrates that were prepared identically and looked similar to those obtained before corrosion. Frames C, F, I, L, and O were obtained after corrosion at 1.0 V for 1 min on the same substrates shown in the before-corrosion images.

The STM image of the naked Au(111) surface after corrosion at 800 mV (Figure 6B) shows that the surface becomes rougher, revealing several new Au terrace levels, as it dissolves downward into the Au in a stepwise manner. Previously, Magnussen et al. studied the dissolution of Au(111) by Br$^-$ with ECSTM and observed step-flow etching of the surface.[45] The naked Au(111) surface after corrosion at 1.0 V (Figure 6C) is somewhat smoother than when it was etched at 800 mV. This is often the case when etching surfaces at higher overpotentials for shorter times.[46]

The Au/C11CH$_3$ surface after corrosion at 800 mV is rougher than the initial surface and characterized by numerous 2.0–12-nm-deep pits. Figure 6E is a representative image of the surface showing two pits that are 2.0–3.0-nm deep and 830–900-nm wide. This type of pitting corrosion usually occurs at defect sites within a protective film[47–49] and often leads to surfaces that are rougher than those corroding in the absence of a protective coating (Figure 6B). Although these deep pits are the most noticeable surface features, there is also an increase in step density throughout the image, suggesting dissolution along step edges as well. The Au/C11CH$_3$ surface after corrosion at 1.0 V (Figure 6F) is again much rougher than the corroded naked Au, but there are no well-defined pits as in the image after etching at 800 mV (Figure 6E). The FTIR-ERS data (Figure 5) indicate that there is significant loss of the C11CH$_3$ SAM at this potential, and the CV in Figure 2 is similar to that of naked Au after only five scans. This stripping of the SAM might explain why the surface corrodes more smoothly without the appearance of large pits.

The Au/C15CH$_3$ surface after corrosion at 800 mV (Figure 6H) contains a few small pits (20–80-nm wide and 0.3–1.5-nm deep); however, there is no indication of dissolution along step edges, and the surface is mostly passivated: the addition of four CH$_2$ units to the alkyl chain of the SAM clearly makes a dramatic difference in corrosion resistance.[50] After corrosion at 1.0 V the Au/C15CH$_3$ surface (Figure 6I) contains numerous pits and is severely roughened. Increasing the potential by 200 mV reduces the ability of the C15CH$_3$ to passivate the Au from Br$^-$, and as in the case of Au/C11CH$_3$ corrosion at 800 mV (Figure 6E), pitting occurs. The majority of pits contain a deep core (10–20-nm deep and 150–250-nm wide) surrounded by a shallower corroded region. This suggests that corrosion initially occurs within the core and then proceeds laterally outward after loss and disordering of the monolayer. The smooth regions of the surface between the pits are thought to contain the ordered monolayer. The density and depth of the pits are greater than those on the Au/C11CH$_3$ surface in Figure 6E, but they are not as wide.

The Au/C10COOH surface after corrosion at 800 mV (Figure 6K) is characterized by roughened step edges,

---

(45) Magnussen, O. M.; Ocko, B. M.; Wang, J. X.; Adzic, R. R. *J. Phys. Chem.* **1996**, *100*, 5500–5508.

(46) West, J. M. *Electrodeposition and Corrosion Processes*, 2nd ed.; Van Nostrand Reinhold Company: London, 1971; pp 106–118.

(47) Bosich, J. F. *Corrosion Prevention for Practicing Engineers*; Barnes & Noble: New York, 1970; pp 40–43.

(48) Bakhvalov, G. T.; Turkovskaya, A. V. *Corrosion and Protection of Metals*, 1st ed.; Pergamon Press Ltd.: Oxford, 1965; p 322.

(49) Wranglen, G. *An Introduction to Corrosion and Protection of Metals*, 1st ed.; Chapman and Hall Ltd.: London, 1985; p 288.

(50) Laibinis, P. E.; Whitesides, G. M. *J. Am. Chem. Soc.* **1992**, *114*, 9022–9028.

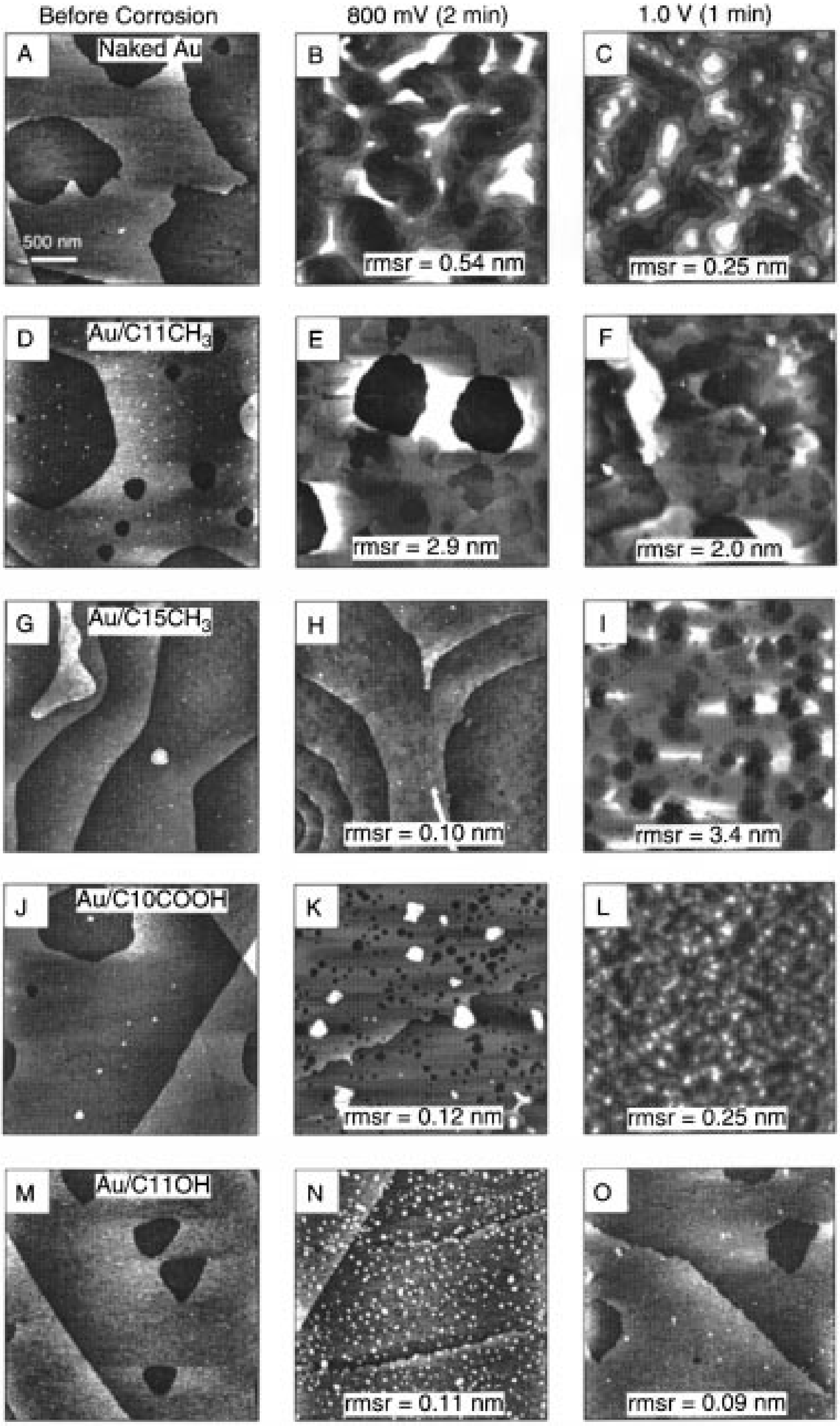

Figure 6. 3 μm × 3 μm STM images of (A−C) Naked Au, (D−F) Au/C11CH$_3$, (G−I) Au/C15CH$_3$, (J−L) Au/C10COOH, and (M−O) Au/C11OH. Within each row, the first image was obtained before corrosion, the second image was obtained after corrosion at 800 mV for 2 min, and the third image was obtained after corrosion at 1.0 V for 1 min. The first and third images in each row were obtained in different regions of the same sample. The second image in each row was obtained on a separate sample that was treated identically and looked similar to the first image in each row. The aqueous electrolyte solution contained 10 mM KBr + 0.1 M HClO$_4$. The bias was 300 mV, and the tunneling current was 150 pA for all images. The gray scale represents a height of 2 nm in all frames except B (z = 6 nm), C (z = 4 nm), E (z = 20 nm), F (z = 30 nm), I (z = 40 nm), and L (z = 5 nm).

islands, and several pits that are one Au atom deep. The surface dissolves rather smoothly compared to the naked Au and Au/C11CH$_3$ surfaces at the same potential. The Au/C10COOH surface after corrosion at 1.0 V (Figure 6L) contains a larger density of steps and is rougher than when dissolved at 800 mV, but it is still smooth when compared to the CH$_3$-terminated SAM surfaces. The Au/C11OH surface (Figure 6N) also corrodes smoothly at 800 mV, but it is covered with many small circular islands (10−40-nm diameter), whose origin is not fully understood. We speculate that the islands appearing in Figure 6K and N are either pin-sites,[51] which are areas of the surface that are passivated (or pinned down) by strongly adsorbed surface impurities, or regions that are more passivated by the SAM. After corrosion at 1.0 V, the Au/C11OH surface (Figure 6O) remains remarkably smooth and the only noticeable corrosion is minor roughening of the step edges, although it is likely that several layers have smoothly etched away. The numerous small islands that covered the surface after corrosion at 800 mV do not appear.

The STM images in Figure 6 after corrosion at 800 mV correlate well with the voltammetric data shown in Figure 1. For example, the first-scan cyclic voltammogram of Au/C11CH$_3$ indicates initial passivation, followed by a sharp rise in current upon additional scanning. This behavior is consistent with the pitting corrosion shown in the STM image. Little current is observed in the cyclic voltammogram of Au/C15CH$_3$, and there is almost no change in surface morphology in the STM image. The cyclic voltammograms of Au/C10COOH and Au/C11OH show a gradual increase in the current as the potential increases and greater monolayer stability on subsequent scans compared to those of Au/C11CH$_3$. This is consistent with the smooth corrosion observed in the STM images of these surfaces. Accordingly, these materials may find applications in the electropolishing industry as a means to produce smooth metal finishes.[46]

The STM data of the surfaces after corrosion at 1.0 V correlate well to the voltammetry shown in Figure 2 and the spectroscopic data in Figure 5. The important result is that, even at high overpotentials, the monolayers capable of hydrogen-bonding are more passivating and lead to less pitting corrosion than the methyl-terminated SAMs. Pitting is highly undesirable because it leads to sudden and unpredictable failures of metal structures; therefore, coatings that promote slow, uniform corrosion can be beneficial.[47]

Although COOH- and OH-terminated SAMs contain more defects than CH$_3$-terminated SAMs,[18] our data indicate they protect Au surfaces from corrosion in Br$^-$ solutions more effectively. Electrochemical data indicate better passivation of the electrode by the hydrophilic SAMs compared to the hydrophobic SAMs. The IR data suggest that all of the monolayers become disordered and orient more parallel to the surface after corrosion. This orientation effect is more prevalent in the hydrophilic SAMs but also occurs with the hydrophobic SAMs. The STM data reveal that the hydrophobic surfaces are extremely rough and contain pits after corrosion, while the hydrophilic surfaces contain monolayer-high Au pits or islands and are quite smooth. The details of the corrosion mechanism are undoubtedly complicated; however, we provide two models in the following discussion that are fully consistent with the data already discussed.

Chart 1

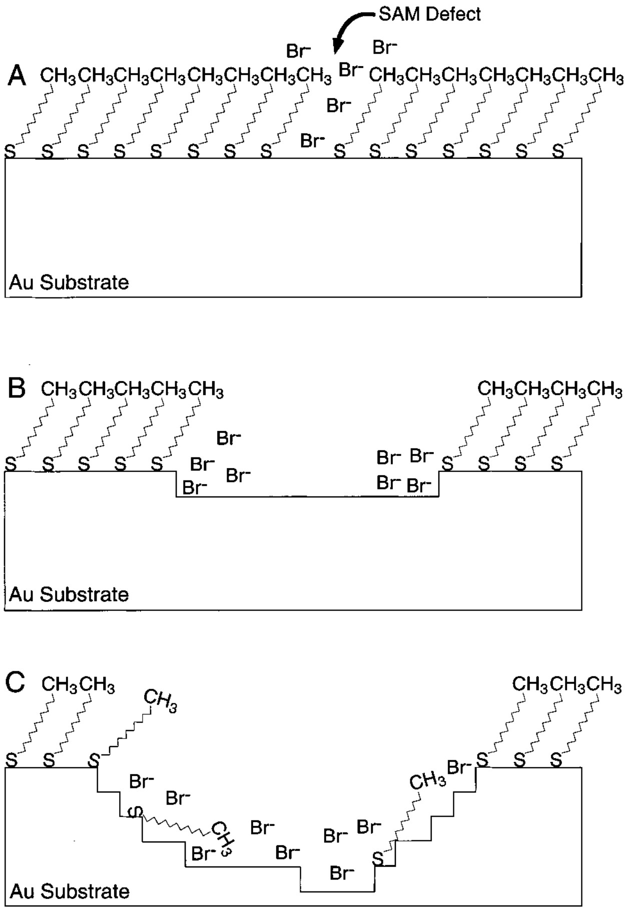

Au surfaces modified with CH$_3$-terminated SAMs undergo pitting corrosion. This occurs because there are defects within the monolayer where Br$^-$ can access the Au and begin etching (frame A of Chart 1). A pit forms in the Au surface and initially expands preferentially within the plane of the Au surface because step edge atoms have higher reactivity than terrace atoms (frame B of Chart 1). Desorption of some thiols accompanies the Au dissolution. At higher potentials, corrosion proceeds in all dimensions, causing the pits to become deeper and wider. Additional thiols desorb from the surface, and others reorient more parallel to the surface plane. This produces regions of disordered thiols in and around the vicinity of the pits and ordered thiols between pits. This proposed mechanism is not in full agreement with that of Scherer et al., who in a recent ECSTM study of *n*-alkanethiol-modified Cu(100) surfaces found that the corrosion mechanism in an etch pit is similar to that on a bare surface and concluded that the pits are therefore absent of thiols.[27] The identity of the chemical species within and near pits is a difficult one, however, and conclusive results will certainly require additional work.

Corrosion of the Au surfaces modified with hydrophilic SAMs (Chart 2) is markedly different than that of those modified with methyl-terminated SAMs. Corrosion of the OH- and COOH-terminated SAMs also begins at defects in the monolayer (frame A of Chart 2). A pit forms and expands along the surface plane, but is subsequently covered by thiols that were on the original terrace (frame B of Chart 2). The hydrophilic SAMs are more mobile on the surface compared to hydrophobic SAMs in aqueous environments. Once a full Au monolayer dissolves, all of the molecules are oriented parallel to the surface in a tail-to-tail conformation where they take advantage of hydrogen-bonding between the end groups (frame C of Chart 2). Deep pitting is inhibited because whenever a

---

(51) Suggs, D. W.; Bard, A. J. *J. Am. Chem. Soc.* **1994**, *116*, 10725−10733.

Chart 2

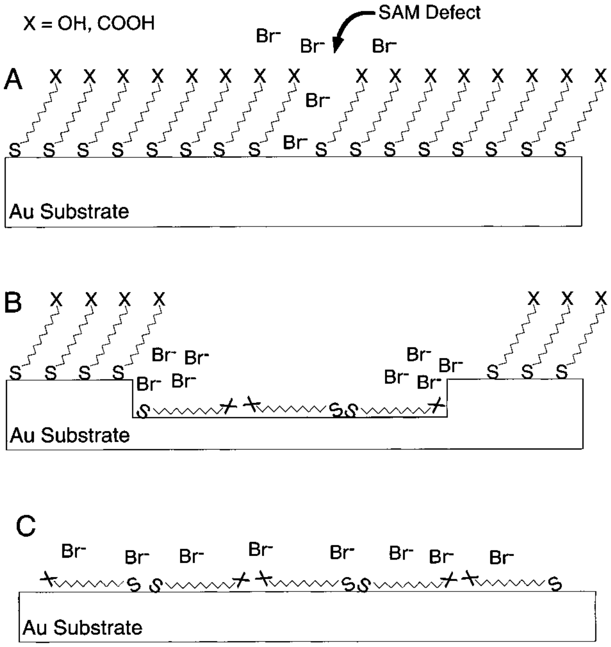

new pit forms, the thiols cover the freshly exposed Au. Thus, corrosion occurs only within the surface plane in a smooth layer-by-layer fashion. The hydrophobic SAM-modified surfaces do not follow this behavior, because they have low surface mobility in aqueous environments and are more prone to stick together due to their hydrophobic nature. Consequently, these surfaces contain deep pits and are characterized by large rmsr values after corrosion.

The flat orientation of thiol molecules has been observed previously by Poirier et al. using scanning tunneling microscopy for monolayers assembled from liquid and vapor phases.[52-54] At low coverages, domains of crystalline islands were observed where the molecules were oriented flat on the surface with their alkyl chains aligned. At saturation coverages, their data indicated that a phase transition occurs and the molecules undergo a structural transition with their alkyl chains oriented more perpendicular to the surface plane. The corrosion model we propose is just the opposite of this assembly process. Initially the molecules are oriented perpendicular to the surface plane and are highly ordered. After corrosion, however, the monolayers become disordered and reorient flat on the surface in a low-density phase.

Summary and Conclusions

We have demonstrated that the SAMs studied (C11CH$_3$, C15CH$_3$, C11OH, C10COOH) suppress corrosion of Au in acidic Br$^-$ solutions compared to naked Au. At low overpotentials (800 mV), the C15CH$_3$ monolayer protects better than the shorter SAMs, consistent with previous reports that longer-chain *n*-alkanethiols form more crystalline, passivating monolayers. However, the C11OH and C10COOH SAMs are superior corrosion barriers compared to the C11CH$_3$ SAM, showing that for similar thicknesses OH and COOH end groups are superior to hydrophobic surfaces for corrosion protection even though it has been shown that they are more easily penetrated by redox-active probe molecules.[18] This means that the ability of the SAM to resist corrosion after it begins is more important than its initial degree of defectiveness. At more positive potentials (1.0−1.1 V), the C11OH and C10COOH SAMs protect better than C11CH$_3$ and, surprisingly, the longer C15CH$_3$ SAMs. The C11OH SAM provides more corrosion resistance than the C10COOH SAM. We conclude that the monolayers reorient parallel to the surface plane during corrosion and that the C11OH- and C10COOH-modified surfaces are more stable and passivating than the C11CH$_3$- and the C15CH$_3$-modified surfaces in this orientation as a consequence of their surface mobility and ability to hydrogen bond.

Further studies examining other important factors affecting the corrosion passivation ability of SAMs such as polymerization, formation of bilayer structures, and placement of SAMs in solution as corrosion inhibitors are currently underway. We hope that such studies will lead to the use of *n*-alkanethiol SAMs as corrosion passivation layers for technologically important applications.

Acknowledgment. We acknowledge the Office of Naval Research for full support of this work. We thank one of the reviewers for suggesting some refinements to the corrosion models illustrated in Charts 1 and 2.

LA971121O

---

(52) Poirier, G. E.; Tarlov, M. J. *Langmuir* **1994**, *10*, 2853−2856.
(53) Poirier, G. E.; Pylant, E. D. *Science* **1996**, *272*, 1145−1148.
(54) Poirier, G. E. *Langmuir* **1997**, *13*, 2019−2026.